

# SWAS and Arecibo observations of H<sub>2</sub>O and OH in a diffuse cloud along the line-of-sight to W51

David A. Neufeld<sup>1</sup>, Michael J. Kaufman<sup>2</sup>, Paul F. Goldsmith<sup>3</sup>, David J. Hollenbach<sup>4</sup> and René Plume<sup>5</sup>

## ABSTRACT

Observations of W51 with *Submillimeter Wave Astronomy Satellite* (SWAS) have yielded the first detection of water vapor in a diffuse molecular cloud. The water vapor lies in a foreground cloud that gives rise to an absorption feature at an LSR velocity of 6 km s<sup>-1</sup>. The inferred water column density is  $2.5 \times 10^{13}$  cm<sup>-2</sup>. Observations with the Arecibo radio telescope of hydroxyl molecules at ten positions in W51 imply an OH column density of  $8 \times 10^{13}$  cm<sup>-2</sup> in the same diffuse cloud. The observed H<sub>2</sub>O/OH ratio of  $\sim 0.3$  is significantly larger than an upper limit derived previously from ultraviolet observations of the similar diffuse molecular cloud lying in front of HD 154368. The observed variation in H<sub>2</sub>O/OH likely points to the presence in one or both of these clouds of a warm ( $T \gtrsim 400$ ) gas component in which neutral-neutral reactions are important sources of OH and/or H<sub>2</sub>O.

*Subject headings:* ISM: abundances – ISM: molecules – ISM: clouds – molecular processes – radio lines: ISM – submillimeter

## 1. Introduction

Since its launch in December 1998, the *Submillimeter Wave Astronomy Satellite* (SWAS; Melnick et al. 2000) has detected water vapor in more than 70 molecular clouds by means

---

<sup>1</sup>Department of Physics & Astronomy, The Johns Hopkins University, 3400 North Charles Street, Baltimore, MD 21218

<sup>2</sup>Department of Physics, San Jose State University, One Washington Square, San Jose, CA 95192

<sup>3</sup>NAIC, Department of Astronomy, Cornell University, Ithaca, NY 14853

<sup>4</sup>NASA Ames Research Center, MS 245-3, Moffett Field, CA 94035

<sup>5</sup>Department of Physics & Astronomy, University of Calgary, 2500 University Drive N.W., Calgary, Canada

of observations the  $1_{10} - 1_{01}$  transition of ortho- $\text{H}_2\text{O}$  (e.g. Snell et al. 2000; Ashby et al. 2000; Neufeld et al. 2000a). While emission-line observations form the core of the SWAS program on interstellar water vapor, absorption-line observations are possible toward a few bright continuum sources; these include Sagittarius B2 (Neufeld et al. 2000b; hereafter N00), Sagittarius A, W49, and W51. Absorption-line observations typically probe the water vapor abundance in several kinematically-distinct foreground clouds lying along the line-of-sight to the source (e.g. N00). Under typical interstellar conditions, most water molecules are in the lower state of the  $1_{10} - 1_{01}$  transition (i.e. in the ground state of ortho-water); thus absorption line observations have the distinct advantage of yielding water vapor column densities that are insensitive both to the physical conditions in the absorbing cloud and to the assumed rate coefficients for collisional excitation of water. Typically, the  $\text{H}_2^{16}\text{O}$  absorption line is very optically-thick, yielding only a lower limit on the water column density, but observations of *optically-thin* absorption by the  $\text{H}_2^{18}\text{O}$  isotopologue (less abundant by a factor of 250–500) have led to a quantitative determination of the water column densities in foreground clouds along the Sgr B2 sight-line (N00).

In this *Letter*, we report the results of similar observations carried out towards the star-forming region W51. The results are particularly intriguing, because they provide our first detection of a  $\text{H}_2^{16}\text{O}$  absorption line which is of only *moderate* optical depth. This feature, observed at an LSR velocity  $\sim 6 \text{ km s}^{-1}$ , originates in a diffuse foreground cloud in the which the water column density is small. This cloud has previously been detected by means of 21 cm absorption-line observations (Koo 1997): the inferred HI column density is  $\sim 10^{21} \text{ cm}^{-2}$ .

Spaans et al. (1998; hereafter S98) have argued that measurements of OH and  $\text{H}_2\text{O}$  column densities in diffuse clouds provide a valuable probe of the chemistry of interstellar oxygen molecules; in particular, the OH/ $\text{H}_2\text{O}$  abundance ratio serves to constrain the branching ratio for the dissociative recombination of the molecular ion  $\text{H}_3\text{O}^+$ , a crucial parameter in chemical models for both diffuse and dense molecular clouds. Accordingly, we have used the Arecibo Observatory (AO) to carry out OH absorption line observations toward the same source, the results of which are also presented here.

The observations and data reduction are described in §2 below, and the observational results presented in §3. In §4 we discuss the derived water and OH column densities and the constraints that they place upon the oxygen chemistry in molecular clouds.

## 2. Observations

Our SWAS observations of W51 were carried out during the period 1999 April 16 – 2001 April 19 with the  $3.3' \times 4.5'$  elliptical SWAS beam centered at position  $\alpha = 19^{\text{h}} 23^{\text{m}} 43.^{\text{s}}0$ ,  $\delta = 14^{\circ}30'38''$  (J2000). All the data were acquired in standard nodded observations (Melnick et al. 2000) and were reduced using the standard SWAS pipeline. The total on-source integration time was 58.6 hours.

AO observations of the 1612, 1665, 1667, and 1720 MHz lines of OH were obtained on 2001 November 30 and 2001 December 3 towards the SWAS-observed position and nine offset positions of widely varying continuum flux. The goal of observing OH towards these offset positions was to allow inferences to be drawn about the line excitation temperatures (see §3.2 below). The offsets and on-source integration times for each observed position are given in Table 1, all positional offsets being expressed relative to the SWAS-observed position. The AO data were obtained in a series of standard nodded observations in which the source and reference positions were alternately observed for a period of 5 minutes each. The reference position was chosen to have an R.A. offset of  $-5 (\cos \delta)$  minutes of time so that the source and reference positions were observed over identical tracks in azimuth and elevation. Calibration measurements were carried out using the noise diode after each source/reference position pair, and calibration observations of an astronomical continuum source were performed at the beginning of each day’s observations.

## 3. Results

### 3.1. SWAS observations of water vapor

Figure 1 shows the complete spectrum of the  $1_{10} - 1_{01}$  556.936 GHz transition of  $\text{H}_2\text{O}$  obtained by SWAS toward W51. The continuum antenna temperature,  $T_{AC}^*$ , measured toward W51 was 0.35 K (double sideband), corresponding to a 550 GHz continuum flux density of  $2.5 \times 10^3$  Jy. The quantity plotted in Figure 1 is the ratio of flux density to continuum flux density, given by  $[T_A^* - 0.5 T_{AC}^*] / 0.5 T_{AC}^*$  under the assumption that the sideband gains are equal. The SWAS beam size is  $3.3' \times 4.5'$  (FWHM) at 550 GHz. The fitted line at  $v_{\text{LSR}} \sim 6 \text{ km s}^{-1}$  is the best-fit absorption line for a cloud that is assumed to completely cover the source. The derived cloud parameters are a line center optical depth  $\tau_0$  of 1.5, a Doppler parameter<sup>6</sup>  $b$  of  $1.5 \text{ km s}^{-1}$ , and cloud LSR velocity of  $6.0 \text{ km s}^{-1}$ . Under

---

<sup>6</sup>The Doppler parameter  $b$  is defined (as usual) such that the optical depth drops by a factor  $e=2.718\dots$  at a velocity shift  $b$  from line center. The corresponding FWHM obtained from a Gaussian fit to the absorption

the conditions typical of diffuse interstellar clouds, the population in the  $1_{10}$  rotational state of water is very small and thus the effects of stimulated emission on the  $1_{10} - 1_{01}$  optical depth can be neglected. The column density of water in the  $1_{01}$  state is straightforwardly obtained as  $1.9 \times 10^{13} \text{ cm}^{-2}$ . If the ortho-para ratio for water is 3, the implied total water column density is  $2.5 \times 10^{13} \text{ cm}^{-2}$ . The water abundance relative to HI is  $\sim 10^{-8}$ .

### 3.2. Arecibo observations of OH

Figure 2 shows the OH spectra obtained at AO towards the ten positions observed in W51. These spectra show the ratio of beam-averaged brightness temperature,  $T_B$ , to continuum brightness temperature,  $T_{BC}$ . The beam-averaged brightness temperature of the radiation incident upon the AO antenna is computed according to  $T_B = T_A/\eta_A + T_{\text{CMB}}$ , where  $T_A$  is the antenna temperature,  $\eta_A \sim 0.8$  is the aperture efficiency – including atmospheric losses, as determined from calibration observations of an astronomical continuum source – and  $T_{\text{CMB}} = 2.73 \text{ K}$  is the temperature of the cosmic background radiation (which is “chopped out” by our observing procedure). The size of the Arecibo main beam is  $\sim 2.6' \times 3.0'$  (FWHM) at 1666 MHz.

The continuum brightness temperatures,  $T_{BC}$ , measured for each position are shown in Table 1, along with the measured equivalent width,  $W_v$  – in units of  $\text{km s}^{-1}$  – for each of the observed OH lines. Here,  $W_v$  is defined as  $\int (T_B - T_{BC})/T_{BC} dv$ , so that a negative value of  $W_v$  implies an absorption line and a positive value an emission line. Because of strong radio frequency interference, the 1720 MHz line strength could be measured reliably only toward the SWAS-observed (0,0) position where the absolute line strength was largest.

The results shown in Table 1 imply that the ratio of equivalent widths departs greatly from the 1:5:9:1 value expected in local thermodynamic equilibrium (LTE) for  $W_v(1612) : W_v(1665) : W_v(1667) : W_v(1720)$ . In particular, the 1665 MHz / 1667 MHz absorption line ratio is considerably smaller than the LTE value and the 1612 MHz / 1667 MHz ratio considerably larger. Moreover, the 1720 MHz line is observed in emission toward the (0,0) position, indicating the presence of weak maser amplification.

For lines of small optical depth, the equivalent width is related to the OH column density and the excitation temperature,  $T_{ex}$ , by the expression

$$W_v = 0.45 k [N(\text{OH})/10^{14} \text{ cm}^{-2}] [T_{ex}/\text{K}]^{-1} [1 - T_{ex}/T_{BC}] \text{ km s}^{-1} \quad (1)$$

---

line is  $3.4 \text{ km s}^{-1}$ .

where  $k = \frac{1}{9}$ ,  $\frac{5}{9}$ , 1 and  $\frac{1}{9}$  respectively for the 1612, 1665, 1667 and 1720 MHz transitions. The ratios and signs of the equivalent widths observed toward the (0,0) position imply that  $T_{ex}(1720) < 0 < T_{ex}(1612) < T_{ex}(1667) < T_{ex}(1665)$ . Assuming that all the excitation temperatures are small compared to  $T_{BC}$  at the (0,0) position (i.e. small compared to 500 K), we find the ratio of excitation temperatures to be  $T_{ex}(1612) : T_{ex}(1665) : T_{ex}(1667) : T_{ex}(1720) = 0.18 : 1.79 : 1 : -0.29$ .

Unfortunately, because the equivalent widths are a function of *two* unknowns –  $N(\text{OH})$  and  $T_{ex}$  – the OH column density and excitation cannot be derived independently for any given sight-line. However, as we argue below, the variation of the equivalent widths with the background continuum brightness temperature,  $T_{BC}$ , for the ten sight-lines we observed, provides a strong argument that the entire region is covered by a large foreground cloud in which the OH column density and excitation are nearly constant. This in turn allows us to derive an estimate of  $N(\text{OH})$ .

In Figure 3 (upper panel), we show the equivalent widths measured for each transition and each observed position as a function of the background continuum brightness temperature,  $T_{BC}$ . We note immediately that the equivalent width of the 1612 MHz transition shows rather little variation over the entire set of observed positions;  $W_v(1612)$  lies within 30% of  $0.08 \text{ km s}^{-1}$  for every sight-line that we observed. Referring to equation (1), we see that the near-constancy of  $W_v$  argues strongly that  $N(\text{OH})$  and  $T_{ex}$  are nearly constant and that  $T_{ex}$  is small compared to 6 K, the smallest  $T_{BC}$  for any sight-line that we observed. In principle, of course,  $N(\text{OH})$  and  $T_{ex}$  could show large variations from one position to another, but it would seem highly improbable that such variations could conspire to yield a right-hand-side for equation (1) that is nearly constant. Therefore, we shall henceforth assume that the OH column density and excitation are nearly the same towards each of the ten positions we have observed.

It is also apparent from Figure 3 that the equivalent widths of the 1665 MHz and perhaps the 1667 MHz transition appear to show a systematic decline in those sight-lines of smallest continuum brightness; this decline allows the line excitation temperatures to be estimated. In Figure 3 (lower panel), we plot the ratio of equivalent widths for the 1665 and 1612 MHz transitions, again as a function of the background brightness temperature. The solid curve shows the best fit to the data, for a model in which the 1612 and 1665 excitation temperatures are assumed to be constant and in the 0.1:1 ratio inferred for the (0,0) position. The best fit curve is obtained for  $T_{ex}(1665) = 7 \text{ K}$ . Adopting this value for  $T_{ex}(1665)$ , we infer from equation (1) and the observed 1665 MHz equivalent width that the OH column density is  $8 \times 10^{13} \text{ cm}^{-2}$  towards the SWAS-observed (0,0) position.

## 4. Discussion

Because of the relative simplicity of the chemical networks involved, diffuse molecular clouds provide a useful laboratory for testing astrochemical models; in particular, the  $\text{H}_2\text{O}/\text{OH}$  abundance ratio serves as a valuable probe of the chemical network that produces oxygen-bearing molecules (S98). One key uncertainty in that network concerns the dissociative recombination of  $\text{H}_3\text{O}^+$  with electrons, and specifically the fraction of such recombinations that produce water,  $f_{\text{H}_2\text{O}}$ , a quantity for which two laboratory groups have obtained highly discrepant results. According to results obtained in the flowing afterglow experiment of Williams et al. (1996), a fraction  $f_{\text{OH}} = 0.65$  of dissociative recombinations of  $\text{H}_3\text{O}^+$  lead to OH, a fraction  $f_{\text{H}_2\text{O}} = 0.05$  to  $\text{H}_2\text{O}$ , and the remaining fraction  $f_{\text{O}} = 1 - f_{\text{OH}} - f_{\text{H}_2\text{O}}$  to O. A different experimental technique (Vejby-Christensen et al. 1997), which made use of the ASTRID heavy-ion storage ring in Denmark, yielded significantly different results (Jensen et al. 2000), *viz.*  $f_{\text{OH}} : f_{\text{H}_2\text{O}} : f_{\text{O}} = 0.74 \pm 0.02 : 0.25 \pm 0.01 : 0.013 \pm 0.005$ . Similar results (although with larger error bars) were obtained (Neau et al. 2000) from the CRYRING heavy-ion storage ring facility; they were  $f_{\text{OH}} : f_{\text{H}_2\text{O}} : f_{\text{O}} = 0.78 \pm 0.08 : 0.18 \pm 0.05 : 0.04 \pm 0.06$ ,

Taken together with the ground-based observations of OH that we obtained at Arecibo, the SWAS observations of W51 imply an  $\text{H}_2\text{O}/\text{OH}$  abundance ratio  $\sim 0.3$  in the diffuse cloud that is responsible for the  $v_{\text{LSR}} = 6 \text{ km s}^{-1}$  feature. Considering the uncertainties in our determination of the  $\text{H}_2\text{O}$  and (particularly) the OH column densities, we estimate the  $\text{H}_2\text{O}/\text{OH}$  ratio to be uncertain by a factor  $\sim 2$ . In comparing the observed  $\text{H}_2\text{O}/\text{OH}$  abundance ratio with theoretical predictions, we have used the steady-state photodissociation region (PDR) model of Kaufman et al. (1999), modified so as to treat the case of a finite slab illuminated from two sides. Because  $\text{H}_2$  and CO are photodissociated following line absorption, their photodissociation rates are reduced by self-shielding. In order to treat correctly the effects of self-shielding for radiation incident upon *both* sides of the slab, the  $\text{H}_2$  and CO abundances must be obtained by an iterative method.

### 4.1. Standard models of cold diffuse clouds

In Figure 4, we show the predicted  $\text{H}_2\text{O}$  and OH column densities for a variety of *astrophysical* parameters: the total visual extinction through the cloud,  $A_V$ , in magnitudes; the illuminating UV field,  $G_0$ , in units of the Habing field; and the cosmic ray ionization rate,  $\zeta_{\text{cr}}$ . All results apply to an assumed cloud density,  $n_H$ , of 100 H nucleons per  $\text{cm}^3$ . The temperature is calculated from considerations of thermal balance and is  $\sim 30$  K at the cloud center. Filled squares apply to models with  $f_{\text{OH}} : f_{\text{H}_2\text{O}} : f_{\text{O}} = 0.75 : 0.25 : 0.0$  (values suggested by the ASTRID storage ring experiment), while filled triangles apply to models

with  $f_{\text{OH}} : f_{\text{H}_2\text{O}} : f_{\text{O}} = 0.65 : 0.05 : 0.30$  (suggested by the flowing afterglow experiment). The different astrophysical parameters for each plotted data point are described in the figure caption. Black circles represent the column densities observed toward W51 and HD 154368.

A striking feature of Figure 4 is that although the  $\text{H}_2\text{O}$  and OH column densities depend strongly on the assumed astrophysical parameters, their *ratio* is determined primarily by the assumed branching ratio  $f_{\text{H}_2\text{O}}$  and shows almost no dependence upon  $A_V$ ,  $G_0$ , or  $\zeta_{\text{cr}}$ . This behavior can be understood by means of a simple “toy” model, in which we assume OH and  $\text{H}_2\text{O}$  to be formed by dissociative recombination of  $\text{H}_3\text{O}^+$  and destroyed by photodissociation. The expected  $\text{H}_2\text{O}/\text{OH}$  ratio is given by

$$\frac{n(\text{H}_2\text{O})}{n(\text{OH})} = \frac{\zeta_{\text{OH}}}{\zeta_{\text{H}_2\text{O}}} \times \frac{f_{\text{H}_2\text{O}}}{f_{\text{OH}} + f_{\text{H}_2\text{O}}} \sim 0.69 \times \frac{f_{\text{H}_2\text{O}}}{f_{\text{OH}} + f_{\text{H}_2\text{O}}} \quad (2)$$

where  $\zeta_{\text{OH}} = 3.5 \times 10^{-10} G_0 \exp(-1.7 A_V) \text{ s}^{-1}$  and  $\zeta_{\text{H}_2\text{O}} = 5.1 \times 10^{-10} G_0 \exp(-1.8 A_V) \text{ s}^{-1}$  are the assumed photodissociation rates for OH and  $\text{H}_2\text{O}$  (Roberge et al. 1991).<sup>7</sup> Equation (2) yields  $\text{H}_2\text{O}/\text{OH}$  abundance ratios of 0.172 and 0.049 respectively for the branching ratios assumed for the filled squares and triangles in Figure 4. These ratios are shown by dashed lines in Figure 4, and do indeed yield good agreement with results from the full steady-state PDR model. The assumption of chemical steady-state is justified by the fact that the photodissociation timescale for OH is only  $\sim 100 \exp(1.7 A_V)/G_0$  years.

Given standard models for cold diffuse clouds, the observed  $\text{H}_2\text{O}/\text{OH}$  abundance ratio of  $\sim 0.3$  in W51 is *consistent* with the case  $f_{\text{OH}} : f_{\text{H}_2\text{O}} : f_{\text{O}} = 0.75 : 0.25 : 0$  and clearly *inconsistent* with the case  $f_{\text{OH}} : f_{\text{H}_2\text{O}} : f_{\text{O}} = 0.65 : 0.05 : 0.30$ . Thus – if interpreted using standard models for cold diffuse clouds – the observed  $\text{H}_2\text{O}/\text{OH}$  abundance ratio argues for the laboratory results obtained in the ASTRID storage ring experiment and against those obtained in the flowing afterglow experiment.

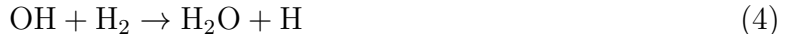
This conclusion, however, is different from that obtained by S98, who used ultraviolet absorption line observations with the Goddard High Resolution Spectrometer of HST to place an upper limit of only 0.06 ( $3\sigma$ ) on the  $\text{H}_2\text{O}/\text{OH}$  ratio in an entirely different diffuse cloud, which lies in front of the star HD 154368. Based upon these observations, S98 argued for a *low* value of  $f_{\text{H}_2\text{O}}$  that is inconsistent with the ASTRID storage ring experiment. The puzzling discrepancy between the observed  $\text{H}_2\text{O}/\text{OH}$  abundance ratio in these two diffuse clouds may point to the importance of additional production mechanisms for OH or  $\text{H}_2\text{O}$  that do not involve the dissociative recombination of  $\text{H}_3\text{O}^+$ . This possibility is addressed in §4.2 below.

---

<sup>7</sup>The quantity  $f_{\text{H}_2\text{O}}$  appears with  $f_{\text{OH}}$  in the denominator of the second term on the right-hand-side, because photodestruction of  $\text{H}_2\text{O}$  results in the formation of OH.

#### 4.2. Enhanced-temperature models of diffuse molecular clouds

It has long been recognized (e.g. Elitzur & de Jong 1978) that neutral-neutral reactions provide an alternate production route to OH and H<sub>2</sub>O. The reactions



possess activation barriers that make them negligibly slow at the low temperatures typical of diffuse interstellar clouds; at temperatures above  $\sim 300$  K, however, they become important production mechanisms for OH and H<sub>2</sub>O (Neufeld, Lepp & Melnick 1995). If even a small fraction of the gas in the W51 6 km s<sup>-1</sup> and/or the HD 154368 cloud were sufficiently warm – as a result of a weak shock, for example – then neutral-neutral reactions might perturb the OH and H<sub>2</sub>O column densities.

To investigate this possibility, we have obtained model predictions for PDRs in which the temperature has been fixed at a variety of temperatures between 100 and 1500 K. The results are represented by the magenta locus in Figure 4; they were obtained for the astrophysical parameters adopted by S98 for the HD 154368 cloud –  $A_V = 2.65$  mag,  $n_H = 325$  cm<sup>-3</sup>,  $G_0 = 3$  – but for a branching ratio  $f_{\text{H}_2\text{O}} = 0.25$  and a cosmic ray ionization rate of  $1.8 \times 10^{-17}$  cm<sup>-3</sup>. The OH and H<sub>2</sub>O column densities are both clearly enhanced by neutral-neutral reactions. At moderate temperatures, the H<sub>2</sub>O/OH ratio decreases because the large O/OH ratio makes reaction (3) more important than (4). At temperatures higher than  $\sim 600$  K, however, the effect on the ratio is reversed, and the H<sub>2</sub>O/OH ratio is *increased* by neutral-neutral reactions.

The results obtained in enhanced-temperature models suggest a way out of the puzzle posed by the discrepant OH/H<sub>2</sub>O ratios measured in the W51 6 km s<sup>-1</sup> and HD 154368 clouds. If these clouds possess small (but differing) amounts of warm gas, then the OH/H<sub>2</sub>O abundance ratios could differ (even though the value of  $f_{\text{H}_2\text{O}}$  must, of course, be identical in both clouds). We are unaware of any observations that rule out the presence of small amounts of warm gas in these sources; indeed, the presence of such gas in diffuse clouds is predicted by certain models that seek to explain the anomalously-high CH<sup>+</sup> abundances observed in many diffuse clouds as resulting from the effects of turbulence or weak shocks<sup>8</sup> (e.g. Joulain et al. 1998, Flower & Pineau des Forets 1998, and references therein).

---

<sup>8</sup>Depending upon the geometry, velocity shifts of the OH and H<sub>2</sub>O lines relative to the lines of other species (e.g. HI) might be an observational signature of a shock production mechanism. The velocity shifts can be very small, however, if the shock propagates at an oblique angle to the line-of-sight or if multiple shocks are present in the beam. Thus, the absence of any such signature in the W51 6 km s<sup>-1</sup> cloud does not argue strongly against the production of OH and H<sub>2</sub>O in shocks.



Unfortunately – as discussed above – the effect of warm gas upon the  $\text{H}_2\text{O}/\text{OH}$  ratio depends critically upon the gas temperature – and even switches sign at  $T \sim 600$  K. Thus, if warm gas is present, the observed  $\text{H}_2\text{O}/\text{OH}$  ratio cannot even be used to derive a limit upon  $f_{\text{H}_2\text{O}}$ . For example, if  $\sim 5\%$  of the gas in HD 154368 were at  $\sim 500$  K, then the observations of OH and  $\text{H}_2\text{O}$  in that source could be reconciled with the large branching ratio  $f_{\text{H}_2\text{O}} = 0.25$  derived in §4.1 above. Alternatively, if  $\sim 0.3\%$  of the gas in the W51 cloud were at  $T \sim 700$  K, then the observed  $\text{H}_2\text{O}/\text{OH}$  ratio would be consistent with the lower limit on  $f_{\text{H}_2\text{O}}$  inferred previously by S98.

To summarize, the discrepancy between the  $\text{H}_2\text{O}/\text{OH}$  ratio reported here for the W51  $6 \text{ km s}^{-1}$  cloud and that reported previously for the HD 154368 cloud (S98) suggests that a component of warm ( $T \gtrsim 400$ ) gas is present in one or both of these sources. The presence of this warm component makes it difficult to determine observationally the branching ratio for the dissociative recombination of  $\text{H}_3\text{O}^+$  with electrons to form OH and  $\text{H}_2\text{O}$ . Our new observations of W51 cast doubt upon the conclusion of S98 that the branching ratio to  $\text{H}_2\text{O}$  is small, but do not allow the branching ratio to be determined definitively.

This work was supported NASA’s SWAS contract NAS5-30702. We gratefully acknowledge the excellent support of the telescope operators at the Arecibo Observatory. The Arecibo Observatory is operated by the National Astronomy and Ionosphere Center under a Cooperative Agreement with the National Science Foundation.

## REFERENCES

- Ashby, M. L. N. et al. 2000, *ApJ*, 539, L115.
- Elitzur, M. & de Jong, T. 1978, *A&A*, 67, 323.
- Flower, D. R. & Pineau des Forets, G. 1998, *MNRAS*, 297, 1182.
- Jensen, M. J. et al. 2000, *ApJ*, 543, 764.
- Joulain, K., Falgarone, E., Des Forets, G. P., & Flower, D. 1998, *A&A*, 340, 241.
- Kaufman, M. J., Wolfire, M. G., Hollenbach, D. J., and Luhman, M. L. 1999, *ApJ*, 527, 795
- Koo, B. 1997, *ApJS*, 108, 489.
- Melnick, G. J. et al. 2000, *ApJ*, 539, L77.
- Neau, A., Al Khalili, S., Rosen, S., et al. 2000, *J. Chem. Phys.*, 113, 1762.
- Neufeld, D.A., Lepp, S., & Melnick 1995, *ApJS*, 100, 132
- Neufeld, D. A. et al. 2000, *ApJ*, 539, L107.
- Neufeld, D. A. et al. 2000, *ApJ*, 539, L111 (N00).
- Roberge, W. G., Jones, D., Lepp, S., & Dalgarno, A. 1991, *ApJS*, 77, 287.
- Snell, R. et al. 2000, *ApJ*, 539, L101.
- Spaans, M., Neufeld, D., Lepp, S., Melnick, G. J., & Stauffer, J. 1998, *ApJ*, 503, 780 (S98).
- Vejby-Christensen, L., Andersen, L.H., Heber, O., Kella, D., Pedersen, H.B., Schmidt, H.T., & Zafman, D. 1997, *ApJ*, 483, 531
- Williams, T.L., Adams, N.G., Babcock, L.M., Herd, C.R., & Geoghegan, M. 1996, *MNRAS*, 282, 413

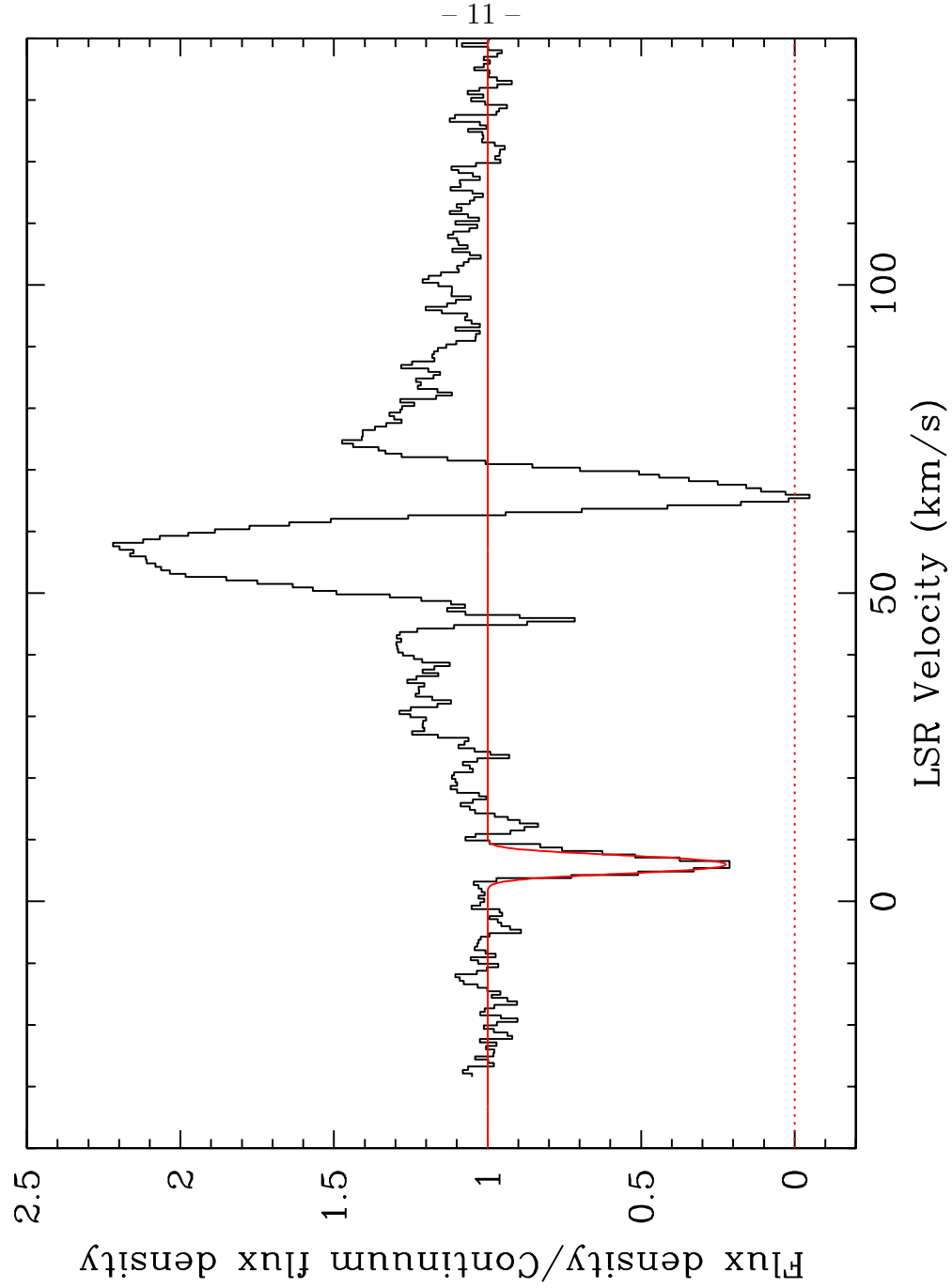


Fig. 1.— Water vapor spectra obtained toward W51 by the Submillimeter Wave Astronomy Satellite. The figure shows the  $1_{10} - 1_{01}$  pure rotational transition of  $\text{H}_2^{16}\text{O}$  near 557 GHz.

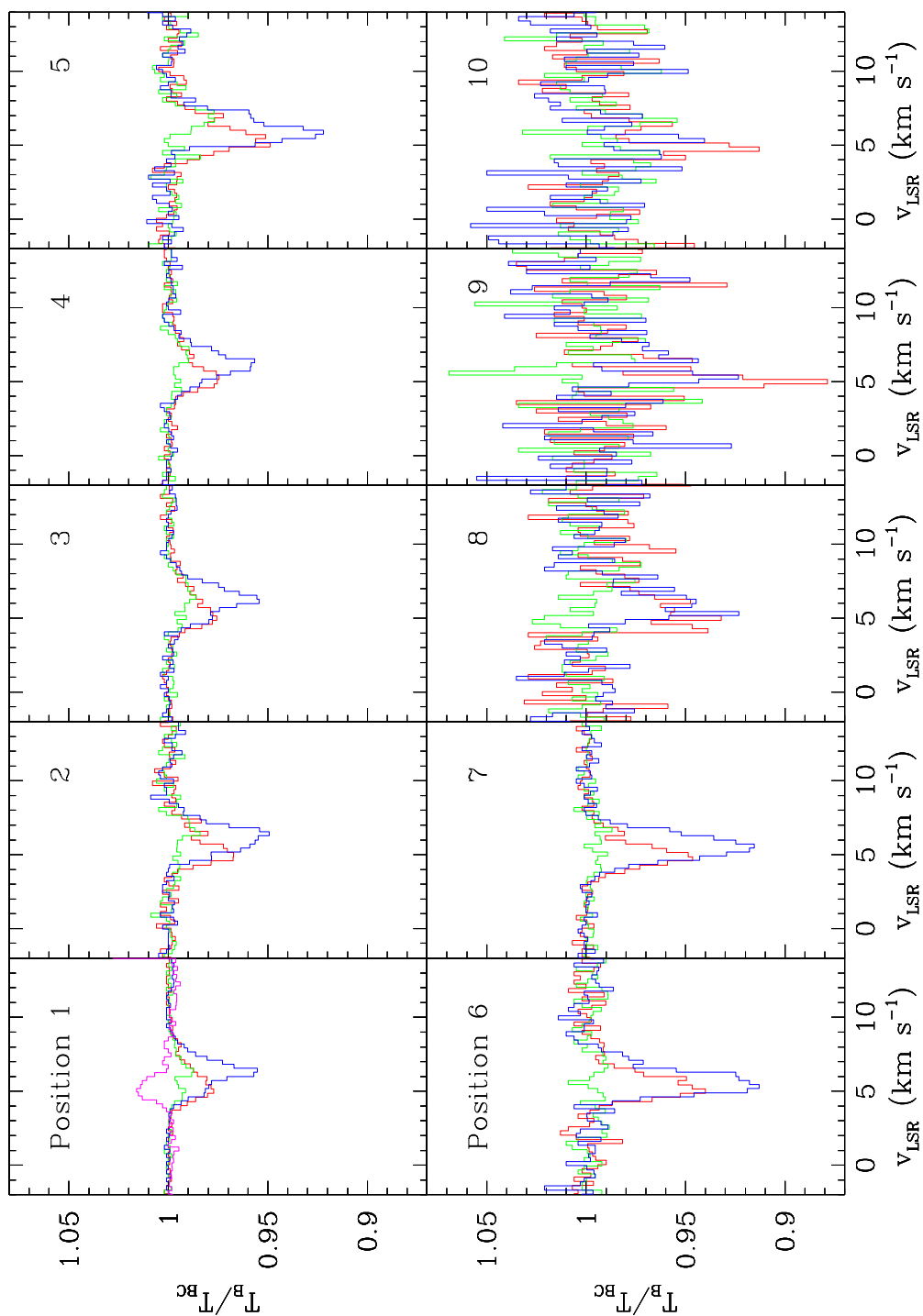


Fig. 2.— OH spectra obtained toward ten positions in W51. The red, green, blue and magenta curves respectively show the 1612, 1665, 1667, and 1720 MHz transitions.

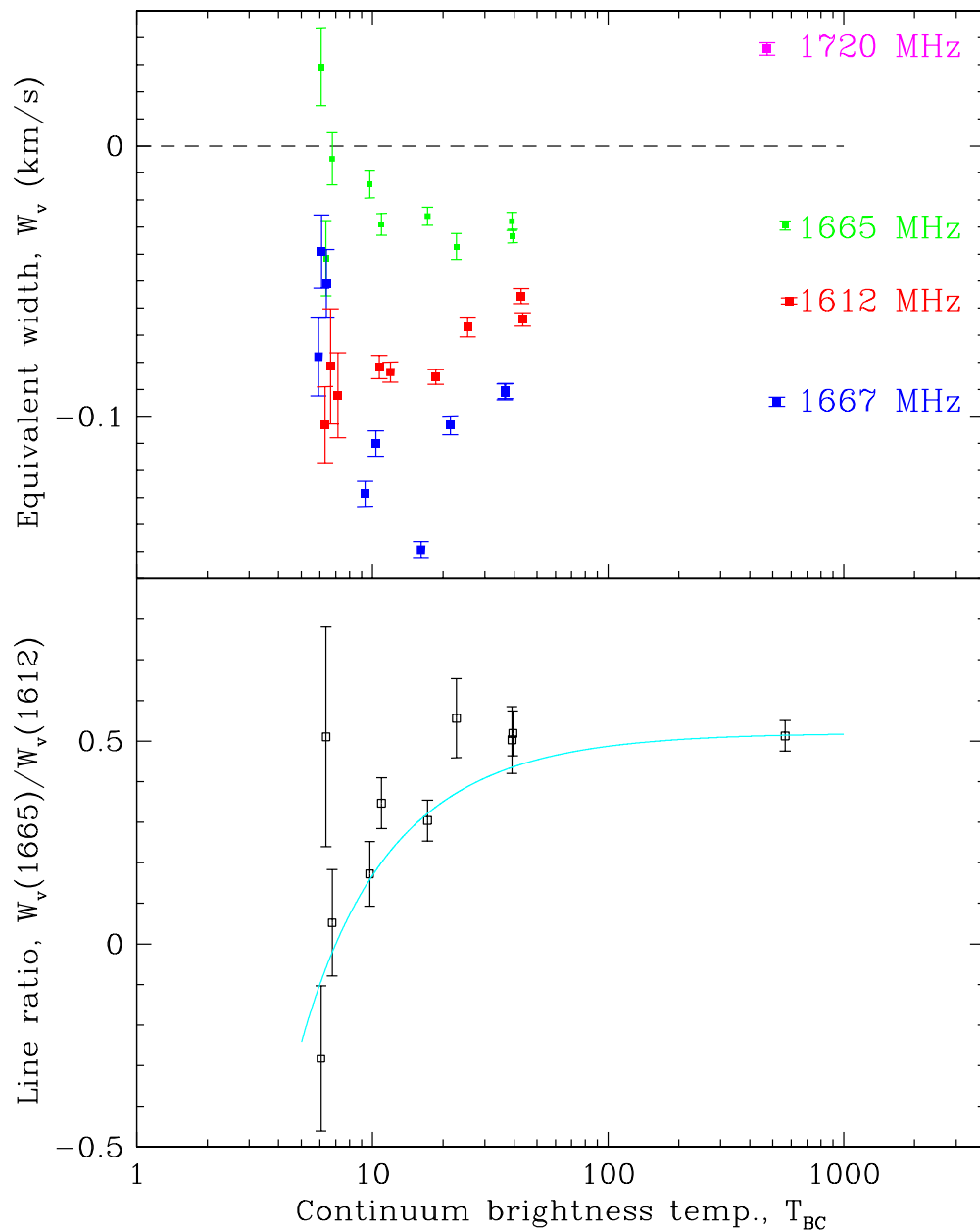


Fig. 3.— OH equivalent widths observed toward ten positions in W51 (upper panel), as a function of continuum brightness temperature at each position. The lower panel shows the ratio of the equivalent widths for the 1665 MHz and 1612 MHz transitions. The curve refers to a fitted model in which the foreground OH column density and excitation is assumed to be the same for all observed positions (see text for the best-fit model parameters).

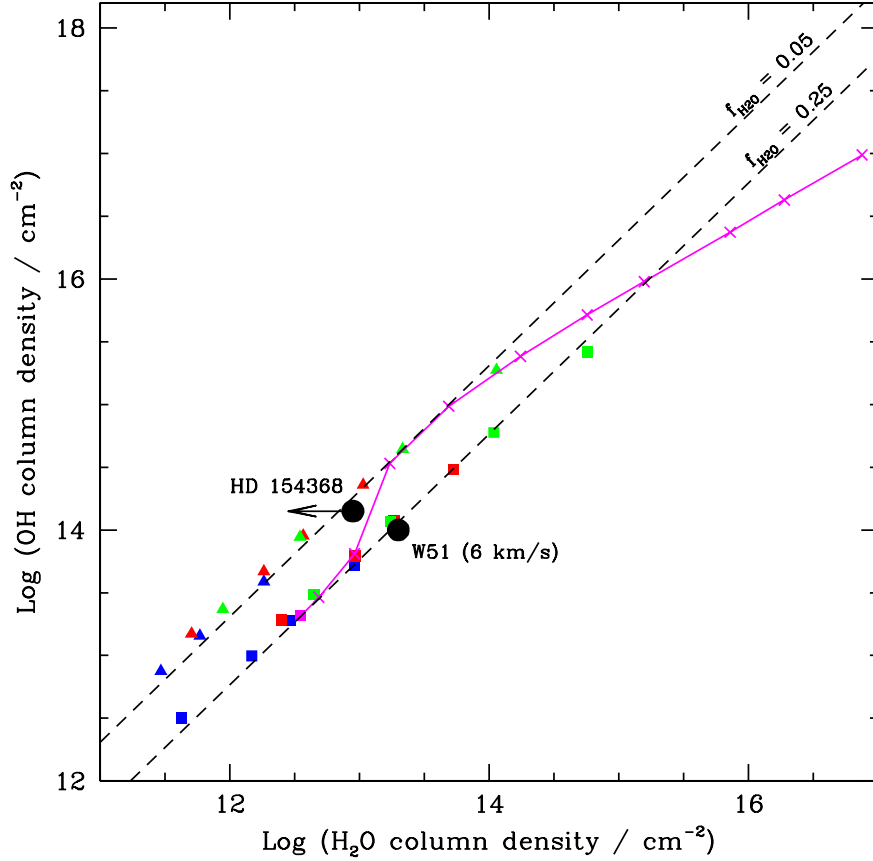


Fig. 4.— OH and H<sub>2</sub>O column densities predicted by a photodissociation model. Results have been obtained for two different assumptions about the branching ratio for dissociative recombination of H<sub>3</sub>O<sup>+</sup>; filled squares apply to models with  $f_{\text{OH}} : f_{\text{H}_2\text{O}} : f_{\text{O}} = 0.75 : 0.25 : 0.0$  (results from the ASTRID storage ring experiment), while filled triangles apply to models with  $f_{\text{OH}} : f_{\text{H}_2\text{O}} : f_{\text{O}} = 0.65 : 0.05 : 0.30$  (flowing afterglow experiment). Red symbols shows the results of models in which the incident UV field,  $G_0$ , is 5 and the cosmic ray ionization rate,  $\zeta_{cr}$ , is  $1.0 \times 10^{-16} \text{ s}^{-1}$ . Blue and green symbols apply respectively to the cases ( $G_0 = 5, \zeta_{cr} = 1.8 \times 10^{-17} \text{ s}^{-1}$ ) and ( $G_0 = 1, \zeta_{cr} = 1.0 \times 10^{-16} \text{ s}^{-1}$ ). In each case, results were obtained for total cloud extinctions,  $A_V$ , of 1, 2, 3, and 4 (from left to right as the points appear in the figure). The black dashed lines show the H<sub>2</sub>O/OH ratios of 0.172 and 0.049 obtained for the two assumed branching ratios using the toy model described in the text. The magenta locus shows the results of enhanced temperature models (see text): from left to right, the points refer to a model in which the temperature is calculated self-consistently (filled square;  $T \sim 30 \text{ K}$  at cloud center) and then (crosses) to models in which the assumed temperature is fixed at 100, 300, 400, 450, 500, 550, 600, 700, 800, and 1500 K.

TABLE 1  
OH observations toward W51

Position	Offset <sup>a</sup>	Time <sup>b</sup> (s)	$T_{\text{BC}}$ <sup>c</sup> (K)	$W_v(1612)$ <sup>d</sup> (km s <sup>-1</sup> )	$W_v(1665)$ (km s <sup>-1</sup> )	$W_v(1667)$ (km s <sup>-1</sup> )	$W_v(1720)$ (km s <sup>-1</sup> )
1	(0, 0)	600	542.8	-0.057 (0.001)	-0.029 (0.002)	-0.095 (0.002)	+0.036 (0.002)
2	(-1.3, -8.3)	600	22.1	-0.067 (0.004)	-0.037 (0.005)	-0.103 (0.003)	
3	(+4.0, -3.3)	600	38.1	-0.064 (0.003)	-0.033 (0.003)	-0.091 (0.003)	
4	(-4.2, +2.2)	600	37.8	-0.056 (0.003)	-0.028 (0.003)	-0.091 (0.003)	
5	(+7.2, -11.8)	1200	10.7	-0.084 (0.004)	-0.029 (0.004)	-0.110 (0.005)	
6	(-11.0, +6.7)	1200	9.5	-0.082 (0.004)	-0.014 (0.005)	-0.129 (0.005)	
7	(-13.4, -8.3)	1200	16.6	-0.085 (0.003)	-0.026 (0.003)	-0.149 (0.003)	
8	(-11.0, +11.7)	600	6.6	-0.092 (0.016)	-0.005 (0.010)	-0.051 (0.013)	
9	(-11.0, +16.7)	300	6.0	-0.103 (0.014)	+0.029 (0.014)	-0.078 (0.015)	
10	(-11.0, +21.7)	300	6.2	-0.082 (0.021)	-0.042 (0.014)	-0.039 (0.014)	

<sup>a</sup> Offset ( $\alpha \cos \delta, \delta$ ) in ' relative to  $\alpha = 19^{\text{h}} 23^{\text{m}} 43^{\text{s}}.0$ ,  $\delta = 14^{\circ} 30' 38''$  (J2000)

<sup>b</sup> On-source integration time

<sup>c</sup> Beam-averaged continuum brightness temperature at 1666 MHz

<sup>d</sup> Line equivalent width (< 0 for absorption line), with statistical errors in parentheses